Int J CARS (2013) 8:937–944
DOI 10.1007/s11548-013-0831-9

ORIGINAL ARTICLE

Accuracy analysis in MRI-guided robotic prostate biopsy

Helen Xu · Andras Lasso · Peter Guion · Axel Krieger · Aradhana Kaushal · Anurag K. Singh · Peter A. Pinto · Jonathan Coleman · Robert L. Grubb III · Jean-Baptiste Lattouf · Cynthia Menard · Louis L. Whitcomb · Gabor Fichtinger

Received: 10 January 2013 / Accepted: 11 March 2013 / Published online: 27 March 2013

Abstract
Purpose To assess retrospectively the clinical accuracy of an magnetic resonance imaging-guided robotic prostate biopsy system that has been used in the US National Cancer Institute for over 6 years.
Methods Series of 2D transverse volumetric MR image slices of the prostate both pre (high-resolution T2-weighted)- and post (low-resolution)- needle insertions were used to evaluate biopsy accuracy. A three-stage registration algorithm consisting of an initial two-step rigid registration followed by a B-spline deformable alignment was developed to capture prostate motion during biopsy. The target displacement (distance between planned and actual biopsy target), needle placement error (distance from planned biopsy target to needle trajectory), and biopsy error (distance from actual biopsy target to needle trajectory) were calculated as accuracy assessment.
Results A total of 90 biopsies from 24 patients were studied. The registrations were validated by checking prostate contour alignment using image overlay, and the results were accurate to within 2 mm. The mean target displacement, needle placement error, and clinical biopsy error were 5.2, 2.5, and 4.3 mm, respectively.
Conclusion The biopsy error reported suggests that quantitative imaging techniques for prostate registration and motion compensation may improve prostate biopsy targeting accuracy.

Keywords Prostate biopsy · Accuracy validation · MRI-guidance · Image registration

H. Xu (✉) · A. Lasso · G. Fichtinger
Queen's University, Kingston, ON, Canada
e-mail: helen@cs.queensu.ca

P. Guion · A. Kaushal · P. A. Pinto
National Institutes of Health, Bethesda, MD, USA

A. Krieger
Children's National Medical Center, Washington, DC, USA

A. K. Singh
Rosewell Park Cancer Institute, Buffalo, NY, USA

J. Coleman
Memorial Sloan-Kettering Cancer Center, New York, NY, USA

R. L. Grubb III
Washington University in St. Louis, St. Louis, MO, USA

J.-B. Lattouf
Centre Hospitalier de L'Universite de Montreal, Montreal, QC, Canada

C. Menard
Princess Margaret Hospital, Toronto, ON, Canada

L. L. Whitcomb · G. Fichtinger
Johns Hopkins University, Baltimore, MD, USA

Introduction

Prostate cancer is the most common form of cancer and the second most common cause of cancer death among American and European men [1]. In 2012, an estimated 241,740 men were diagnosed with prostate cancer and an estimated 28,170 died of this disease [1]. Due to inconclusive results from prostate-specific antigen (PSA) and digital rectum exam (DRE) screening tests, prostate biopsy is the most definitive form of cancer diagnosis. Approximately 1.5 million prostate biopsies are performed annually in the United States [1]. The current standard biopsy procedures use 2D transrectal ultrasound (TRUS) guidance. Since tumors are not visible in ultrasound, in TRUS-guided biopsies, usually six (hence, "sextant

biopsy") to eighteen cores are removed from upper, mid, and lower areas of the left and right sides to obtain a representative sampling of the gland and determine the degree and extent of cancer. There are many problems associated with this non-exhaustive systematic search method for an unknown target. First, the pressure from the transducer probe while imaging causes dynamic prostate deformation throughout the procedure, which can lead to inaccurate needle placement. The location of biopsy is also lost after the procedure, making precise re-biopsy of the same region of the prostate difficult or impossible. TRUS-guided biopsy only has a detection rate of 20–40 % [2,3], and it misses cancer in at least 20 % of the cases [4,5]. Such observations have been seen with no major changes for about a decade [6,7]. Cancers have been routinely missed, resulting in a large number of repeat biopsy cases [8].

The superior soft tissue imaging quality of magnetic resonance imaging (MRI) provides an alternative for biopsy guidance. Possible cancerous regions can be identified on the MR images and therefore allowing target-specific biopsies to be performed at these sites. Due to confined physical space in the scanner and the length of the procedure, robotic assistance is often required. Numerous MRI-compatible biopsy systems were developed for this purpose [9]. The access to prostate tissue under MRI (APT-MRI) system has been used at the US National Cancer Institute (NCI) for over 6 years [10,11] (Fig. 1). The robot is fixated to the patient table and the end that contains the imaging probe with a built-in needle guide is placed inside the patient transrectally. The device is then calibrated to scanner coordinate system, and diagnostic scans are taken. Next, it is remotely controlled to set the desired needle position and angle for a specific biopsy target. The needle is then advanced into the prostate transrectally through the needle guide to acquire tissue samples for histological analysis.

The prostate movement upon needle insertion can be extremely complex since it can deform and dislocate independently from surrounding structures. In addition, patient movement due to discomfort can further complicate the problem. The current system does not take into consideration of these factors, yet the biopsies still need to be sufficiently accurate to hit the intended target in order not to miss the suspected cancerous tissue. This paper reports a retrospective quantitative evaluation of the biopsy accuracy for the APT-MRI robotic biopsy system. In addition, a detailed prostate motion analysis during biopsy is also provided.

Related works

Prostate motion and deformation upon needle insertion have only been studied by a few groups using MR images. Some common approaches include tracking a number of manually identified anatomical landmarks [12] or using surface contours to align the prostate [13,14]. The accuracy of these feature-based methods depends heavily on the user segmentation, which can be inconsistent especially at the apex and base of the prostate gland. Some groups applied biomechanical models to study the organ geometry and boundary constraints [15–17], while others chose image-based methods such as rigid or deformable registration using mutual information and correlation coefficient [18,19]. Biomechanical models also require segmentation and knowledge of material properties, which can be difficult and time consuming. Thus, image-based rigid and deformable registration would be the most suitable for our case. However, due to huge variability in the image quality from the large dataset provided by the NCI, none of the existing method mentioned is capable of accurately determining the transformation between our image pairs with short computation time and little manual interference. We developed an algorithm designed to capture the majority of prostate motion during APT-MRI-guided transrectal biopsy for most of our patient data.

A preliminary study was previously done by our group [20]. This paper presents results from a larger data set and includes several major improvements to the original registration framework. These include: image preprocessing, deformable registration and accuracy validation on all dataset instead of a randomly selected small subset, validation using ground truth, more in-depth statistical analysis, and major decrease in the amount of manual work.

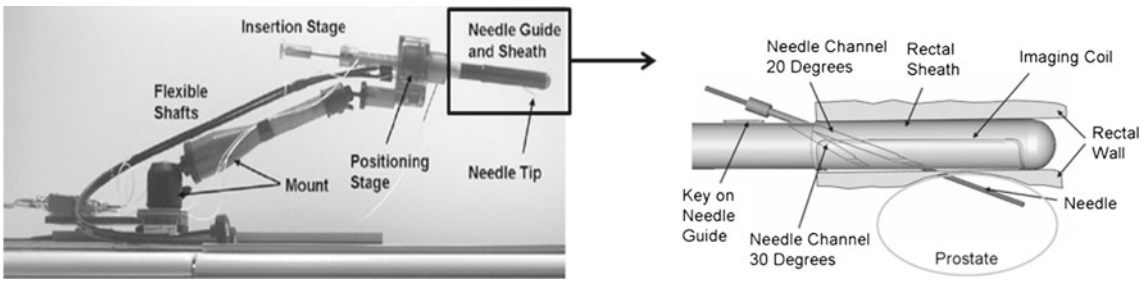

Fig. 1 The APT-MRI robotic biopsy device system used in NCI [6]

Materials and methods

Data acquisition

The MR images were collected from the US National Cancer Institute over a period of 6 years. Although there were variations in the clinical protocol, the following steps were common to all trials. First, a series of 2D high-resolution T2 transverse volumetric image slices covering the whole prostate were acquired with the patient in prone or supine position inside the MRI scanner. From this pre-needle insertion volume, the clinicians select the biopsy target locations in right-anterior-superior (RAS) coordinates, where the origin is approximately the center of the prostate. Once the biopsy target locations are chosen, the APT-MRI device was used to place the biopsy needle transrectally into the prostate to acquire tissue samples. While the needle is still in place, another set of 2D transverse volumetric image slices were obtained to confirm needle placement.

There was an at least 10-min gap between the diagnostic targeting image acquisition and the biopsy needle confirmation image, during which prostate and patient movement may have occurred. Therefore, to obtain the actual biopsy target location, image registration between the pre- and post-needle insertion volumes needs to be performed to account for rigid motion and deformation during the procedure. The resulting transformation from the registration can then be applied to the planned biopsy target to locate its coordinates in the post-needle insertion volume.

Image registration

The data used for registration and biopsy accuracy evaluation are the sets of 2D transverse volumetric image slices of the prostate pre- and post-needle insertion. Developing a registration algorithm to capture the prostate motion and deformation for the majority of the images in the dataset was a difficult task. The images were collected from different clinical trials, using different imaging protocols, by different clinicians, with several different versions of the APT-MRI device. There are large variations in image resolution, field strength, amount of artifacts etc. In addition, the complex prostate movement and deformation due to needle insertion along with patient motion during the procedure further complicate the task. The extent of these motions and deformations also varies from patient to patient. Nonetheless, a computation method that is suitable for most of the cases is needed for retrospective biopsy accuracy analysis. The rest of this section describes our implementation details.

The MR images were first pre-processed to decrease intensity non-uniformity in homogeneous tissue regions using N4ITK (Nick's N3 Insight Toolkit) implementation for MRI bias field correction [21]. This method does not require expert supervision, user interaction, or training, and only has a few user-defined parameters. The two most important parameters are *bias full width at half maximum* (BWHM) and *noise*. BWHM defines the Gaussian that estimates the bias field, and noise specifies the Wiener filter used for field estimation. By experimentation, it was found that BWHM at 0.5 and noise at 0.01 or 0.1 (depending on the image) worked the best for our clinical images. Other parameters had a much smaller influence on the bias correction results.

After pre-processing, a three-stage volume-to-volume registration procedure was developed using ITK [22] to determine the transformation between the pre- and post-needle insertion volumes. This captures the prostate movement, including both dislocation and deformation during biopsy (Fig. 2). The procedure starts with a simple rigid registration of the entire image volume to compensate for prostate motion in coherence with the biopsy device and patient. Next, another rigid step was performed using only the prostate as the region of interest to correct for residual decoupled prostate motion. Finally, a B-spline deformable registration with a grid size of $5 \times 5 \times 5$ was used to fine-tune the alignment and to adjust for tissue deformation that occurred during the procedure. Due to the aforementioned large differences in our images, mutual information was chosen to be the similarity metric. Furthermore, our implementation involved a

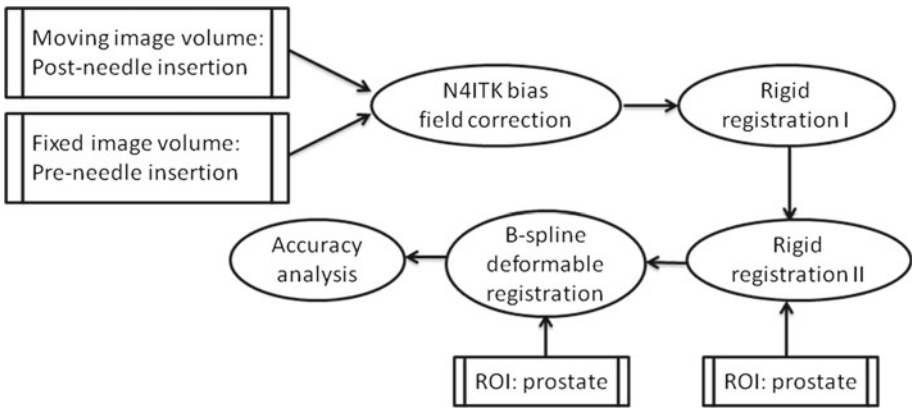

Fig. 2 Workflow of the three-stage registration algorithm between the pre- and post-needle insertion volumes using mutual information

variant of the gradient descent optimizer for versor rigid 3D transform, and an L-BFGS-B (Limited-memory Broyden–Fletcher–Goldfarb–Shannon with simple bounds) optimizer for the deformable component.

In the clinical MR images, the exact correspondence of the prostate anatomy cannot be identified easily. In addition, prostate movement can be decoupled from surrounding organs and bony structures. Therefore, typical validation methods such as using landmarks to evaluate the registration accuracy are not applicable in our case. To validate our registration algorithm, we first generated simulated image volumes by applying known transformations (ground truth) to an existing image volume. The difference between ground truths and the recovered transformations generated by the algorithm from registering simulated volumes with the original volume was calculated. We then proceeded to validate the algorithm on actual clinical image pairs by performing image overlays and evaluating the prostate contour alignment between the resulting volumes with its corresponding fixed volume. This process was done in 3D Slicer, a free open source software package for visualization and image analysis [23]. All of our images in the dataset were verified for its registration accuracy. If the results were off by more than 2 mm, manual registrations were performed.

Biopsy accuracy analysis

To evaluate quantitatively and analyze the biopsy accuracy, we defined and studied the following three terms (Fig. 3):

Target displacement is the distance between planned (pre-needle insertion) and actual (post-needle insertion) biopsy target. The actual target location was obtained by applying the transformation from the registration algorithm to the planned target. To determine whether this dislocation is the same as the needle insertion direction, the displacement was decomposed into two components: one parallel and one orthogonal to the needle vector. A Wilcoxon signed-rank test was conducted to see whether target movement in the needle direction was significantly higher than the orthogonal direction.

Needle placement error is the distance from the planned biopsy target to the biopsy needle trajectory line. This distance indicates how much the robot had missed the intended target, assuming no prostate motion during the biopsy procedure. The needle trajectory line was obtained using two needle tip coordinates from the post-insertion volume. Commonly used titanium needles are not directly visible in MRI, but they generate an artifact in the immediate neighborhood of the needle. Therefore, the true needle position may differ from the artifact position. However, in this particular case, the needle artifact errors are significantly smaller than the errors due to patient motion and tissue deformation [24].

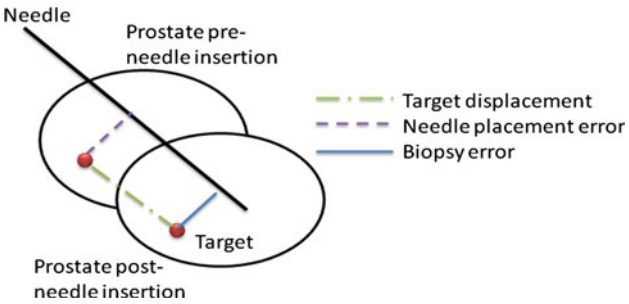

Fig. 3 Illustration of the prostate dislocation during needle insertion and the parameters used in biopsy accuracy analysis

Biopsy error is the distance from the actual biopsy target to the needle trajectory line. This is the most relevant metric for assessing biopsy accuracy, since the length of the tissue core excised by the needle is about 20 mm long; hence, target movement orthogonal to the needle trajectory is of our main concern. To further study the orthogonal component of the displacement, it was separated into RAS coordinates and principle component analysis (PCA) was performed on the data.

Results

Registration accuracy

The patient data selection for this study simply requires available planning and needle confirmation image volumes along with the corresponding planned biopsy target coordinates. A total of 90 biopsies from 24 patients were studied.

The accuracy of the registration procedure was studied in order to provide a bound on biopsy accuracy evaluation. Images from 5 patients were each transformed by a different ground truth. The differences between all of the ground truth and the recovered transformations from the algorithm were less than 1.0 mm. The registration results from all 90 biopsies were validated using the previously discussed image overlay approach. The inaccuracy from the automatic registration was mainly due to poor image quality. After manual adjustments, all registrations were accurate to within 2 mm. Figure 4 shows an example of a prostate surface before and after the automatic registration. The signed-rank test has shown that the results from rigid and deformable registrations were significantly different ($p \approx 0$). However, rigid registrations recovered the majority (88 %) of the transformation.

As part of our validation process, we also manually registered the rectum and pubic bone from some of the images separately to verify whether patient and robotic device motion were different from that of the prostate. We chose to estimate patient motion by measuring the displacement of the pubic

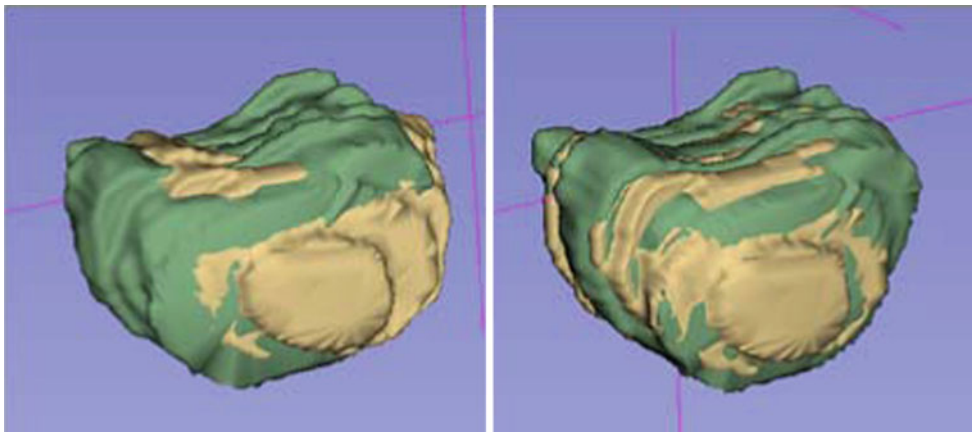

Fig. 4 Prostate contour overlays before (*left*) and after (*right*) the automatic registration

bone, and robotic motion by the displacement of the rectum, since it contains the endorectal imaging probe of the biopsy device. We found that the prostate motion was different from its surrounding structures, and it moved more similar to the bone than that of the rectum.

Biopsy accuracy

The mean, range, and standard deviation for target displacement, needle placement error, and biopsy error are summarized in Table 1. The histograms of these measurements for all 90 biopsies are shown in Fig. 5a–c. Furthermore, target displacements in RAS coordinates are plotted in Fig. 5d–f. Lilliefors tests were conducted and it was found that none of the target displacements, needle placement errors, and biopsy errors are normally distributed. However, the biopsy errors do follow a folded normal distribution ($p = 0.08$).

The parallel (mean 3.1 mm) and orthogonal (mean 3.6 mm) component of the displacement to the needle trajectory was computed and found to be not statistically different ($p = 0.3$) from one another, based on a signed-rank test. For the parallel component, only 32 % of the targets moved toward the needle insertion direction (mean 2.8 mm), and the rest 68 % went in the opposite direction (mean 3.3 mm). Since the biopsy tissue core is about 20 mm in length, it was still able to excise the tissue that had displaced in the direction that is parallel to the needle. A PCA was performed on the orthogonal component in RAS coordinates. The resulting first two principal components ([1, 0.1, −0.1] and [−0.2, 0.9, −0.4]) accounted for 96 % of the data variance.

To study the effect of patient movement on biopsy accuracy, 22 biopsies that contained lateral patient motion (determined by visual inspection of the displacement of rectum and pubic bone in 3D Slicer) greater than 5 mm were grouped separately. Motions larger than 5 mm were suspected to be caused by involuntary patient movements such as pelvis movement or reflexive muscle clenching due to discomfort, which is in nature different from prostate dislocation and deformation caused by the needle. The results for these 22 biopsies alone and the rest of the 68 biopsies are listed in Table 1. The large patient motion caused a 2.1 mm increase in the mean biopsy error. Biopsies performed at the left and right side of the prostate were also analyzed separately. Results show that 43 % of right biopsies had a prostate displacement toward right, and 61 % of left biopsies had displacement toward left.

Discussion

The results from our three-stage registration algorithm allowed for quantitative evaluation of the targeting accuracy for the APT-MRI system as well as prostate motion analysis during biopsy. A clinically significant tumor has a minimum volume of 0.5 cm^3 [25], which correspond to a sphere with a radius of approximately 5 mm. Therefore, the maximum error should be less than 5 mm to not miss

Table 1 The data statistics for accessing biopsy accuracy

	Target displacement (mm)			Needle placement error (mm)	Biopsy error (mm)		
Mean	5.2	4.4*	7.8**	2.5	4.3	3.8*	5.9**
Range	0.9–18	0.9–14.8*	1.6–18**	0.1–10.7	0.2–12	0.2–11.6*	1.7–12**
SD	3.5	3*	3.8**	1.6	2.9	2.8*	2.8**

* Biopsies without the patient movement >5 mm group
** Biopsies only for patient movement >5 mm group

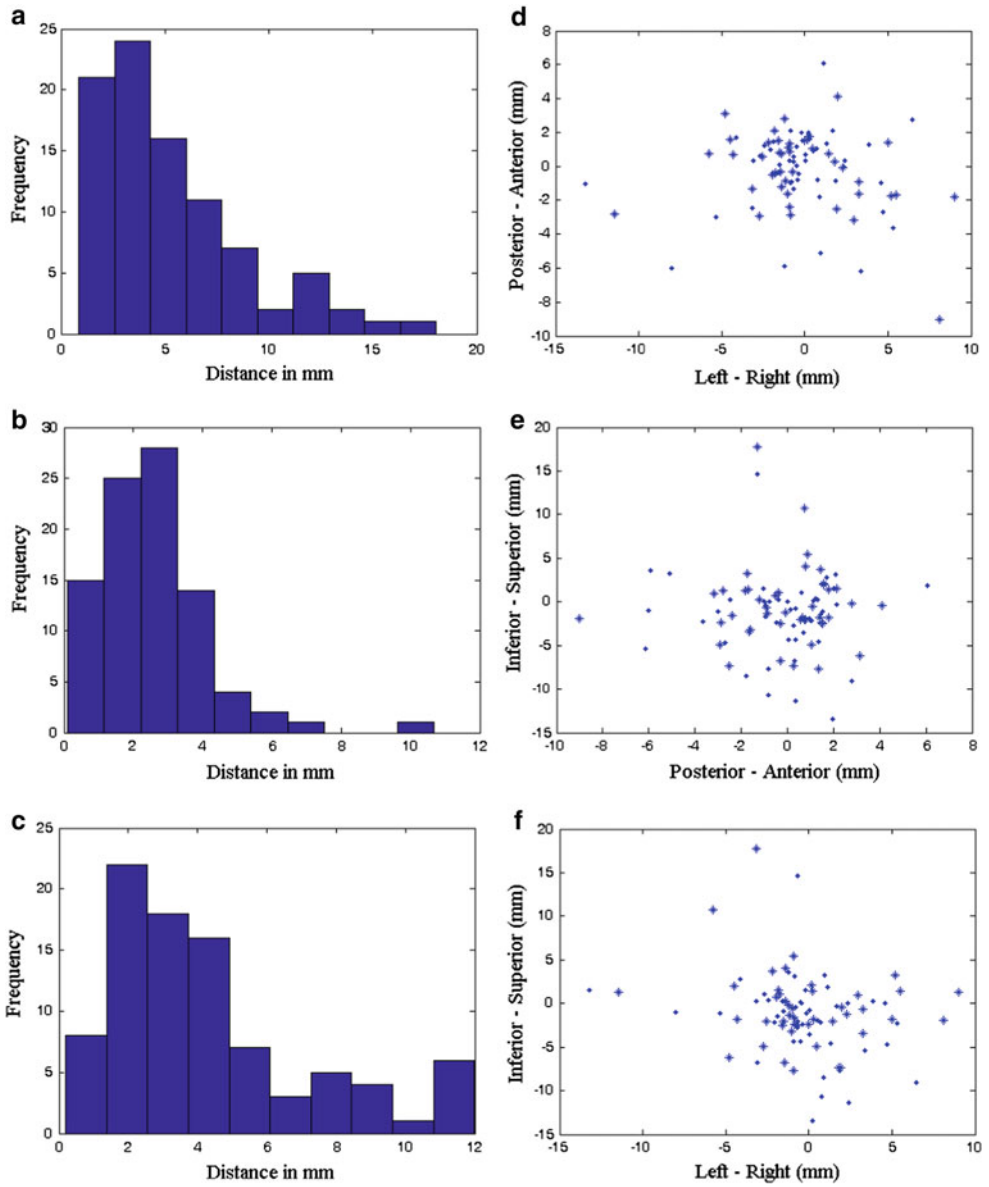

Fig. 5 **a** histogram of target displacements, **b** histogram of needle placement errors, **c** histogram of biopsy errors, **d** axial view of the target displacements, **e** sagittal view of the target displacements, **f** coronal view of the target displacements. *Asterisk* and *dot* represent left and right side biopsy

the targeted region. The targeting accuracy of the APT-MRI system is considered to be technically acceptable, since the mean and standard deviation of its needle placement error are 2.5 and 1.6 mm, respectively (Table 1). This implies that the robotic device was accurate enough to place the needle at the intended biopsy target assuming no prostate movement during the procedure. However, the prostate did dislocate and deform upon needle insertion. Based on the 90 biopsy cases used in this study, the mean prostate displacement was over 5 mm. This resulted in a mean biopsy error of 4.3 mm. Furthermore, 28 % of the biopsies have an error greater than 5 mm, and this error is higher for cases with large patient motion (Table 1). The folded normal distribution of the biopsy errors means that any future errors will have a 95 % probability of falling between two standard deviations (5.8 mm) above 0 mm. To monitor for gross and sudden changes to the prostate location due to patient motion, real-time tracking by plane-to-volume registrations can be used [26].

The biopsy needle was inserted approximately in the superior–anterior direction toward the prostate. However, statistical test indicated that only half of the prostate dislocation was in this direction. The majority of the variance from the other half can be captured by the first two eigenvectors from PCA of the orthogonal component of the displacement.

This implies that the component of prostate dislocations that caused the majority of the biopsy errors can be defined by a plane with vectors [1, 0.1, −0.1] and [−0.2, 0.9, −0.4].

The separate registrations of prostate, rectum, and pubic bone indicated that the prostate was capable of moving independently of its surrounding structures. The reason why its movement was more similar to the pubic bone may be due to the transrectal robotic device limiting rectum movement when the patient moves. The registration results also have shown that even though the majority of prostate motion during biopsy is rigid, there was also a significant amount of deformation caused by the needle insertion process. Therefore, to track the precise target location during biopsy, deformable registration is recommended in addition to rigid registration.

In conclusion, we performed a retrospective accuracy analysis of an MRI-guided robotic prostate biopsy system [6,7] by using a three-stage registration procedure to capture prostate motion during biopsy with an accuracy of 2 mm. The volumetric and soft tissue imaging capabilities of MRI enabled us to identify the needle location in relation to the prostate anatomy. In addition, the registration results allowed for quantitative characterization of prostate dislocation and deformation during transrectal biopsy. It was found that majority of the prostate motion during the procedure was rigid, but there were also a significant amount of deformation during the process. Furthermore, the prostate moved differently from its surrounding structures. The exact amount of these motion and deformation cannot be determined without fiducials or finer volume images. However, even taking into account of the imperfections of our validation framework, the results still suggest that there is a substantial amount of biopsy errors that should not be ignored. Further research on prostate motion and deformation upon needle insertion should be conducted to facilitate the development of motion compensation techniques, which can be incorporated into the clinical protocol to increase biopsy accuracy.

Acknowledgments This work is supported by: US National Institutes of Health (NIH) 5R01CA111288-04 and 5R01EB002963-05, Canadian Ontario Graduate Scholarship (OGS), and Applied Cancer Research Unit program of Cancer Care Ontario with funds provided by the Ontario Ministry of Health and Long-Term Care. Gabor Fichtinger was funded as a Cancer Ontario Research Chair.

Conflict of interest None.

References

1. American Cancer Society (2012) Cancer facts and figures. http://www.cancer.org/acs/groups/content/@epidemiologysurveilance/documents/document/acspc-031941.pdf. Accessed 9 Jan 2013
2. Tempany C, Straus S, Hata N, Haker S (2008) MR-guided prostate interventions. J Magn Reson Imaging 27:356–367
3. Kronz JD, Allan CH, Shaikh AA, Epstein JI (2001) Predicting cancer following a diagnosis of high grade prostatic intraepithelial neoplasia on needle biopsy: data on men with more than one follow-up biopsy. Am J Surg Pathol 25(8):1079–1085
4. Wefer A, Hricak H, Vigneron D, Coakley F, Lu Y, Wefer J, Mueller-Lisse U, Carroll P, Kurhanewicz J (2000) Sextant localization of prostate cancer: comparison of sextant 16 biopsy, magnetic resonance imaging and magnetic resonance spectroscopic imaging with step section histology. J Urol 163(2):400–404
5. Taira AV, Merrick GS, Galbreath RW, Andreini H, Taubenslag W, Curtis R, Butler WM, Adamovich E, Wallner KE (2010) Performance of transperineal template-guided mapping biopsy in detecting prostate cancer in the initial and repeat biopsy setting. Prostate Cancer Prostatic Dis 13(1):71–77
6. Terris MK, Wallen EM, Stamey TA (1997) Comparison of midlobe versus lateral systematic sextant biopsies in the detection of prostate cancer. Urologia Internationalis 59(4):239–242
7. Terris MK (2009) Strategies for repeat prostate biopsies. Curr Urol Rep 10(3):172–178
8. Welch H, Fisher E, Gottlieb D, Barry M (2007) Detection of prostate cancer via biopsy in the medicare-SEER population during the PSA era. J Nat Cancer Inst 99(18):1395
9. Futterer JJ, Barentsz JO (2012) MRI-guided and robotic-assisted prostate biopsy. Curr Opin Urol 22(4):316–319
10. Krieger A, Susil R, Menard C, Coleman J, Fichtinger G, Atalar E, Whitcomb L (2005) Design of novel MRI compatible manipulator for image guided prostate interventions. IEEE Trans Biomed Eng 52(2):306–331
11. Krieger A, Iordachita I, Guion P, Singh AK, Kaushal A, Menard C, Pinto PA, Camphausen K, Fichtinger G, Whitcomb LL (2011) An MRI-compatible robotic system with hybrid tracking for MRI-guided prostate intervention. IEEE Trans Biomed Eng 58(11):3049–3060
12. Kaplan I, Oldenburg NE, Meskell P, Blake M, Church P, Holupk EJ (2002) Real time MRI-ultrasound image guided stereotactic prostate biopsy. Magn Reson Imag 20:295–299
13. Hirose M, Bharatha A, Hata N, Zou KH, Warfield SK, Cormack RA, D'Amico A, Kikinis R, Jolesz FA, Tempany CMC (2002) Quantitative MR imaging assessment of prostate gland deformation before and during MR imaging-guided brachytherapy. Acad Radiol 9(8):906–912
14. Reynier C, Troccaz J, Fourneret P, Dusserre A, Gay-Jeune C, Descotes JL, Bolla M, Giraud JY (2004) MRI/TRUS data fusion for prostate brachytherapy preliminary results. Med Phys 31(6):1568–1575
15. Brock KK, Nichol AM, Ménard C, Moseley JL, Warde PR, Catton CN, Jaffray DA (2008) Accuracy and sensitivity of finite element model-based deformable registration of the prostate. Med Phys 35(9):4019–4025
16. Alterovitz R, Goldberg K, Pouliot J, Hsu ICJ, Kim Y, Noworolski SM, Kurhanewicz J (2006) Registration of MR prostate images with biomechanical modeling and nonlinear parameter estimation. Med Phys 33(2):446–454
17. Misra S, Macura K, Ramesh K, Okamura A (2009) The importance of organ geometry and boundary constraints for planning of medical interventions. Med Eng Phys 31(2):195–206
18. Oguro S, Tokuda J, Elhawary H, Haker S, Kikinis R, Tempany C, Hata N (2009) MRI signal intensity based B-spline nonrigid registration for pre- and intraoperative imaging during prostate brachytherapy. J Magn Reson Imaging 30(5):1052–1058
19. Fei B, Wheaton A, Lee Z, Duerk JL, Wilson DL (2002) Automatic MR volume registration and its evaluation for the pelvis and prostate. Phys Med Biol 47(5):823–838
20. Xu H, Lasso A, Vikal S, Guion P, Krieger A, Kaushal A, Whitcomb LL, Fichtinger G, (2010) MRI-guided robotic prostate biopsy: a

clinical accuracy validation. MICCAI 2010 Beijing, China LNCS 6363/2010, pp 383–391
21. Tustison NJ, Gee JC (2009) N4ITK: Nick's N3 ITK implementation for MRI bias field correction. Insight J. http://hdl.handle.net/10380/3053. Accessed 9 Jan 2013
22. Yoo TS, Ackerman MJ, Lorensen WE, Schroeder W, Chalana V, Aylward S, Metaxes D, Whitaker R (2002) Engineering and algorithm design for an image processing API: a technical report on ITK—the insight toolkit. Stud Health Technol Inform 85:586–592
23. Pieper S, Halle M, Kikinis R (2004) 3D slicer. In: IEEE international symposium on biomedical imaging: from nano to macro, pp 632–635
24. Sang-Eun S, Cho NB, Iordachita II, Guion P, Fichtinger G, Kaushal A, Camphausen K, Whitcomb LL (2012) Biopsy needle artifact localization in MRI-guided robotic transrectal prostate intervention. IEEE Trans Biomed Eng 59(7):1902–1911
25. Ploussard G, Epstein JI, Montironi R, Carroll PR, Wirth M, Grimm MO, Bjartell AS, Montorsi F, Freedland SJ, Erbersdobler A, van der Kwast TH (2011) The contemporary concept of significant versus insignificant prostate cancer. Euro Urol 60:291–303
26. Tadayyon H, Lasso A, Kaushal A, Guion P, Fichtinger G (2011) Target motion tracking in MRI-guided transrectal robotic prostate biopsy. IEEE Trans Biomed Eng 58(11):3135–3142